

Integrated Spectral Energy D istributions and A bsorption Feature Indices of Single Stellar P opulations

Fenghui Zhang,^{1?} Zhanwen Han,¹ Lifang Li,¹ Jarrod R . Hurley²

¹N ational A stronom ical O bservatories/Yunnan O bservatory, the C hinese A cadem y of Sciences, P.O . box 110, Kunming, Yunnan P rovince, 650011, P.R.C.

²D epartment of A strophysics, American M useum of N atural H istory, Central Park West at 79th Street, New York, NY 10024, U SA

20 March 2024

A B S T R A C T

Using evolutionary population synthesis (EPS) we present integrated spectral energy distributions (ISEDs) and absorption-line indices defined by the Lick Observatory image dissector scanner (referred to as Lick/IDS) system, for an extensive set of instantaneous burst single stellar populations (SSPs). The ages of the SSPs are in the range 1 =G yr – 19 and the metallicities $2.3 \leq [Fe/H] \leq 0.2$. Our models use the rapid single stellar evolution (SSE) algorithm of Hurley, Pols & Tout (2000) for the stellar evolutionary tracks, the empirical and semi-empirical calibrated BaSeL-2.0 model of Lejeune, Cuisinier & Buser (1997, 1998) for the library of stellar spectra and empirical fitting functions of Worthey et al. (1994) for the Lick/IDS spectral absorption feature indices.

Applying our synthetic Lick/IDS absorption-line indices to the merit function we obtain the age and the metallicity of the central region of M 32, it can be well interpreted with an instantaneous SSP with an age of ~6.5 G yr and a metallicity similar to solar. Applying the derived age and the metallicity from the merit function to a number of index-index diagrams, we find that the plots of H – Fe5015 and H – Fe5782 are the best index-index diagrams from which we can directly obtain reasonable age and metallicity.

K ey w ords: stars: evolution { galaxies: individual M 32 { galaxies: stellar content.

1 IN T R O D U C T I O N

Age effects often mask metallicity effects in the studies of stellar populations (O'Connell 1976, 1986, 1994; Worthey 1992), and separating them is a cumbersome affair (Renzini 1986; Buzzoni, G ariboldi & M antegazza 1992; Buzzoni, Chincarini & M olinari 1993). The age-metallicity degeneration originates from the fact that increasing either the metallicity or the age makes the integrated spectral energy distribution (ISED) of a single stellar population (SSP) redder (Bressan, Chiosi & Tantalo 1996).

Previous studies showed that it is difficult to break this degeneration only by broad-band colours (Arimoto 1996; Worthey 1994). In order to solve this question, some studies used spectral information, instead of colours only, in the evolutionary population synthesis (EPS) models (Bressan, Chiosi & Fagotto 1994; Bruzual & Charlot 1993; Bruzual 1996, 2003; Buzzoni 1989; Kodama & Arimoto 1997; Tantalo et al. 1996; Vazdekis 1999; Worthey 1994). With the development of these models including spectral information,

the spectral resolution has been improved from about 20 Å to 2 Å (Vazdekis 1999).

Furthermore, these spectral information has been translated to the line strengths either by empirical fitting polynomials (Gorgas et al. 1993; Worthey et al. 1994; Worthey & Ottaviani 1997) or approaches other than the Lick fitting functions (Peletier 1989; Buzzoni 1995). The inclusion of absorption feature indices in EPS models could add the power of diagnostics to the study of stellar populations (Worthey 1994), therefore some studies have included spectral absorption feature indices into EPS models attempting to understand the stellar populations. Some earlier EPS studies contained spectral indices include no metallicity dependence (Bruzual 1983; Tinsley 1972a,b; Tinsley & Gunn 1976) or are otherwise limited in scope (Aaronson et al. 1978; Frogel, Persson & Cohen 1980; Gould 1978; Tripicco & Bell 1992). Recently, the spectral absorption indices have been combined systematically in EPS studies, in those models some model builders use the absorption feature indices at intermediate resolution (9 Å) of Lick system (Bruzual 1996, 2003; Jones & Worthey 1995; Kurth, A ivensleben & Fricke 1999; Peletier 1989; Vazdekis et al. 1996; Vazdekis 1999; Worthey 1994), which has been accepted by many investigators and

? E-mail: gssephd@public.km.yun.cn

widely used in their studies; other model builders use the indices at considerably higher resolution (FWHM $\sim 2\text{\AA}$) in Rose system (Buzzoni et al. 1992, 1993; Gorgas et al. 1993; Rose 1994; Vazdekis 1999, 2001).

SSPs are assemblies of chemically homogeneous and coeval single stars, the star formation history of any stellar system can be described by a superposition of SSP models with different ages and metallicities. Studying SSPs can help us to understand the evolution of clusters and galaxies, the distribution of metallicities, and to quantify the star formation history of the galaxies. In this paper we also investigate SSPs with a systematic and self-consistent set of stellar evolution models by Pols et al. (1998), spectral library {the BaSeL-2.0 model (Lejeune 1997; Lejeune et al. 1997, 1998) and the spectral absorption feature indices of Lick system (Gorgas et al. 1993; Worthey et al. 1994).

The outline of the paper is as follows. In Section 2, we describe our SSPs models and algorithm. In Section 3, we give the results and discussion. In Section 4, we apply the observed spectral indices to the merit function to determine the age and the metallicity for SSP-like assembly. Finally we present the summary and conclusions in Section 5.

2 MODEL DESCRIPTION

2.1 Input physics

In this study we use the stellar evolutionary models of Pols et al. (1998) obtained with the Eggleton stellar evolutionary code (Eggleton 1971, 1972, 1973; Han, Podsiadlowski & Eggleton 1994; Pols et al. 1995) and the empirical and semi-empirical calibrated BaSeL-2.0 stellar spectral library of Lejeune, Cuisinier & Buser (1997, 1998).

Instead of using a tabular form in the previous EPS studies (Schaller et al. 1992; Charbonneau et al. 1993; Mowlavi et al. 1998) we choose the evolutionary models of Pols et al. (1998) in the convenient form of the rapid single star evolution (SSE) package presented by Hurley, Pols & Tout (2000). Except for a set of analytic evolution functions fitted to the Pols et al. (1998) model tracks, the SSE package extends the tracks by including a description of the remnant phases of stellar evolution, such as the white dwarf cooling track, and supplements the models of Pols et al. (1998) by including a prescription for mass loss, which has been neglected by the models of Pols et al. (1998). The detailed descriptions about the stellar evolutionary models of Pols et al. (1998), the SSE package of Hurley et al. (2000) and the BaSeL-2.0 stellar spectra library of Lejeune et al. (1997, 1998) have been presented in Zhang et al. (2002, paper I), so we do not discuss them here. We refer the interested reader to parts 2 and 3 of paper I for them. In this paper the factor (Reimers' mass-loss coefficient, Reimers 1975) is taken to be 1/4 (Renzini 1981; Iben & Renzini 1983; Carraro et al. 1996).

Except for the ISEDs, we will also calculate a series of Lick/IDS (image disector scanner) spectral absorption feature indices. The Lick/IDS indices are the absorption strengths in 'feature' bandpass, and the 'feature' regions are listed in Table 1 of Worthey et al. (1994). In Lick system 21 absorption features are included, six different molecular bands (CN 4150, G band, MgH, MgH + MgB, and two TiO bands) and 14 different blends of atomic absorption lines.

The indices of molecular bands are expressed in magnitudes, the atomic features indices are expressed in angstroms of equivalent width (EW).

The Lick/IDS absorption-line indices are given by a series of empirical fitting functions of Worthey et al. (1994) as a function of T_{eff} , $\log g$, and metallicity [Fe/H]. The effective temperature spans a range 2100 $\leq T_{\text{eff}} \leq 11000$ K and the metallicity is in the range $-1.0 \leq [\text{Fe}/\text{H}] \leq +0.5$. The indices in the Lick system were extracted from the spectra of 460 stars obtained between 1972 and 1984 using the red-sensitive IDS and Cassegrain spectrograph on the 3m Shane telescope at Lick Observatory. The spectra cover the range 4000–6400 Å, with a resolution of $\sim 8\text{\AA}$ (Worthey et al. 1994).

2.2 Model input

For the EPS of an instantaneous burst SSP the main input model parameters are: (i) the initial mass function (IMF), which gives the relative number of stars in different evolutionary stages; (ii) the lower and upper mass cut-offs M_1 and M_u ; (iii) the relative age, τ , of the SSP; and (iv) the metallicity Z of the stars.

We use the IMF of Kroupa, Tout & Gilmore (1993, hereafter KTG). The KTG IMF takes the form

$$(M) = A \begin{cases} 0.035M^{-1.3} & \text{if } 0.08 \leq M < 0.5; \\ 0.019M^{-2.2} & \text{if } 0.5 \leq M < 1.0; \\ 0.019M^{-2.7} & \text{if } 1.0 \leq M < 1; \end{cases} \quad (1)$$

where A is a normalization constant and M is the stellar mass in solar units. The relative number of stars in the mass range $M_1 \leq M \leq M_u$ is $(M)dM$ where (M) is normalized by

$$Z_{M_u} (M) M dM = 1 : \quad (2)$$

Taking the lower and upper mass limits, M_1 and M_u , of the stellar mass range as $0.1M_\odot$ and $120M_\odot$ respectively, gives the normalization constants $A' = 16.4$ for the KTG IMF.

2.3 Algorithm

Once the input physics database is given, we obtain evolutionary parameters such as luminosity L , effective temperature T_{eff} , radius R and mass M for each star in a SSP using the SSE algorithm, transform these evolutionary parameters to stellar flux with the BaSeL-2.0 stellar spectral model, and obtain absorption feature indices of the Lick/IDS system using the fitting functions of Worthey et al. (1994). By the following equations (3–5) we can obtain the integrated monochromatic flux and absorption feature indices for an instantaneous SSP of a particular age and metallicity.

In the following equations, a parameter identified by a capital letter on the left-hand side represents the integrated SSP, while the corresponding parameter in minuscule on the right-hand side is for stars. The integrated monochromatic flux of a SSP is defined as

$$Z_{M_u} F_{\lambda, z} = \int_{M_1}^{M_u} (M) f_{\lambda} dM ; \quad (3)$$

where f_i is the SED of stars with mass M_i and metallicity Z at a relative age of i .

The integrated absorption feature index of the Lick/IDS system is a flux-weighted one. For the i th atomic absorption line, it is expressed in equivalent width (W_i , in Å),

$$W_{i;Z} = \frac{R_{M_u}}{R_{M_1}} \frac{w_i}{f_{i;c}} \frac{(M_i)}{dM_i}; \quad (4)$$

where w_i is the equivalent width of the i th index of stars with mass M_i and metallicity Z at a relative age of i , and $f_{i;c}$ is the continuum flux at the midpoint of the i th 'feature' passband; and for the i th molecular line, the feature index is expressed in magnitude,

$$C_{i;Z} = 2.5 \frac{R_{M_u}}{R_{M_1}} \frac{10^{-0.4c_i}}{f_{i;c}} \frac{(M_i)}{dM_i}; \quad (5)$$

where c_i is the magnitude of the i th index of stars with mass M_i and metallicity Z at age i .

For stars cooler than 3570K, the fitting functions of Worthey et al. (1994) use two completely different sets of coefficients for giants and dwarfs, so we must give a criteria to distinguish them. We adopt the description of Vazdekis et al. (1996) for giants and dwarfs, i.e.,

$$\begin{aligned} &\text{dwarfs; if } \log g < 4.0; \\ &\text{giants; if } \log g > 3.5; \end{aligned} \quad (6)$$

while for stars with gravity in the range $3.5 < \log g < 4.0$, $V - K$ is used to discriminate two classes of stars, i.e.,

$$\begin{aligned} &\text{dwarfs; if } (V - K) < \log g < 6; \\ &\text{giants; if } (V - K) > \log g < 6; \end{aligned} \quad (7)$$

3 RESULTS AND DISCUSSION

In this part we present the ISEDs at intermediate resolution (10Å in the ultraviolet and 20Å in the visible) and the Lick/IDS absorption-feature indices for SSPs over a large range of age and metallicity: 1–19 Gyr and 2.3–[Fe/H] + 0.2. As a check on our models we compare our synthetic ISEDs with those of Worthey (1994, hereafter GW) and that of NGC 6838, and compare our synthetic Lick/IDS absorption-feature indices with the values of Worthey (1994), Vazdekis et al. (1996, hereafter VCPB) and Kurth et al. (1999, hereafter KAF), and those of Galactic and M 31 globular clusters.

3.1 Integrated Spectral Energy Distribution

In Figs. 1 and 2 we give the variation of the intermediate resolution ISED with age and metallicity over a wide wavelength range, $3.3 < \log(\lambda/\text{\AA}) < 5.0$. The flux is expressed in magnitude and is normalized to zero at 2.2 m. Figs. 1 and 2 show that the effects of age and metallicity on the ISEDs are similar, i.e., the ISEDs tend to be redder with increasing age or metallicity in the wavelength region of $3.3 < \log(\lambda/\text{\AA}) < 4.3$.

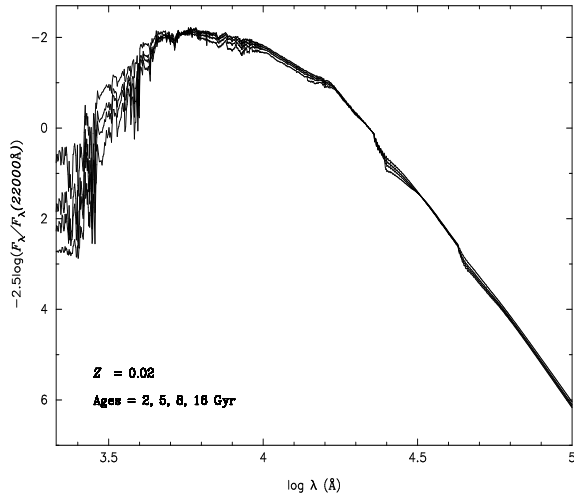


Figure 1. The integrated spectral energy distributions as a function of age for solar metallicity SSPs. From top to bottom the age = 2, 5, 8 and 16 Gyr respectively. The flux is expressed in magnitude and is normalized to zero at 2.2 m.

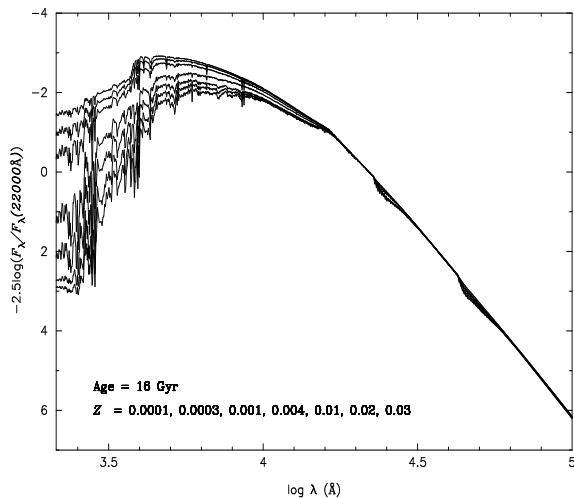


Figure 2. The integrated spectral energy distributions as a function of metallicity for SSPs at age of = 16 Gyr. From top to bottom the metallicity Z is 0.0001, 0.0003, 0.001, 0.004, 0.01, 0.02 and 0.03 respectively. The flux is also expressed in magnitude and is normalized to zero at 2.2 m.

3.1.1 Comparison with the results of previous studies

To test our models we compare our synthetic ISEDs with those of GW for the young ($= 2$ Gyr) and the old ($= 12$ Gyr) SSPs with solar metallicity in the top panels of Figs. 3 and 4, respectively. The ISEDs of GW are based on his work in 1994 and from his private homepage (astro.wsu.edu/worthey/dial/dial.htm), which allows one to obtain ISEDs and the Lick/IDS absorption feature indices for arbitrary mixtures of single-burst SSPs with ages in the range 1–18 Gyr and metallicities in the range [Fe/H] + 0.5 (but not for metallicity [Fe/H] < 0.225 with age < 8 Gyr).

Figs. 3 and 4 show significant disagreement of the ISED in two wavelength regions, the larger one is in the far-ultraviolet region ($\log(\lambda/\text{\AA}) < 3.3$), the minor is in the visi-

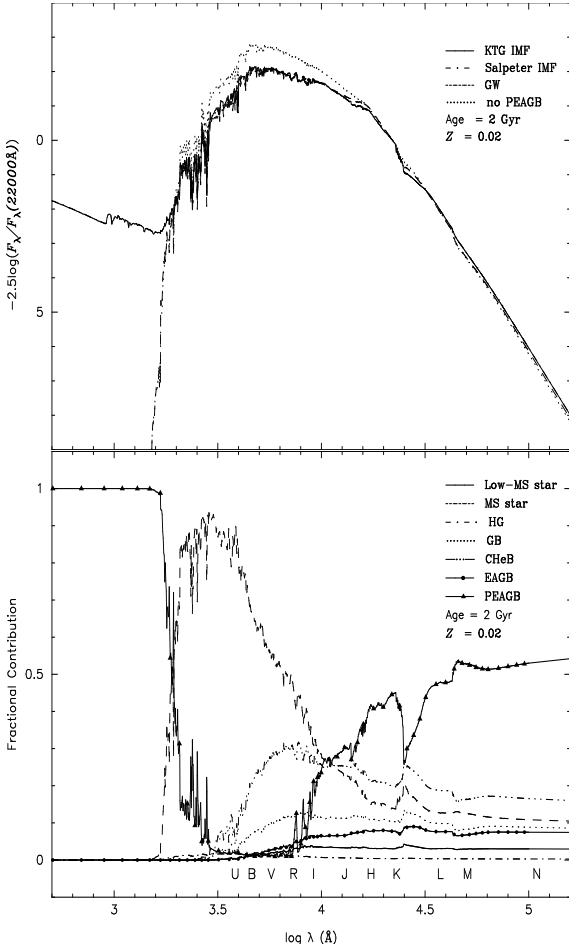


Figure 3. In the top panel comparison of ISEDs for SSPs with age = 2 Gyr and solar metallicity is shown for this work (solid line) and Worthey (dashed line). In order to analyze the discrepancy of ISEDs we also give the ISEDs for our SSPs drawn from the Salpeter IMF with slope = 2.35 (dot-dash line, in the far-ultraviolet region overlapping the ISED with the KTG IMF) and that for our SSPs drawn from the KTG IMF but without PEAGB (see the definition in the text) stars included (dotted line, in the far-ultraviolet region overlapping GW's ISED). The flux is also expressed in magnitude and is normalized to zero at 2.2 m. In the bottom panel the fractional contributions of different evolutionary stage to the total flux is shown for corresponding SSPs. The abbreviations are explained in the text.

ble and infra-red regions (i.e., $3.5 < \log(\lambda/\text{\AA}) < 4.2$). In the first wavelength region our ISED is completely different from that of GW, in the second region this work exhibits bluer continuum than that of GW. Comparing the discrepancy of ISED in the visual and infra-red regions for the young and the old SSPs it seems that this discrepancy in ISED increases with age.

(1) Model Comparison

In order to investigate what actually causes the discrepancy between our ISEDs and those of GW, we first discuss the differences between these two EPS models. This work differs from that of GW by the adoption of

different stellar evolutionary models. We use the stel-

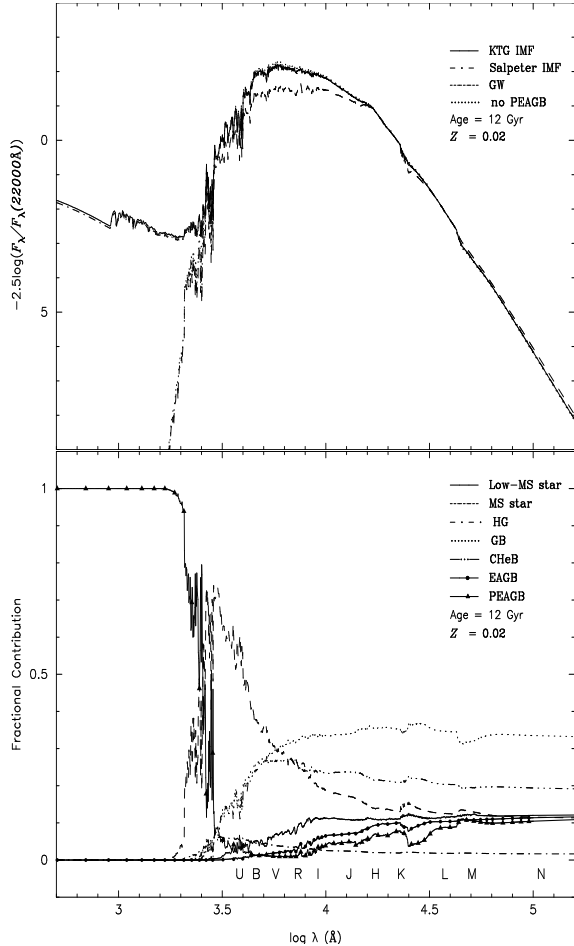


Figure 4. Similar to Fig. 3, but for an age of 12 G yr.

lar evolutionary models of Pols et al. (1998), whereas GW use the stellar evolutionary isochrones by VandenBerg and collaborators (VandenBerg 1985, 1992; VandenBerg & Bell 1985; VandenBerg & Laskarides 1987) and the revised Yale isochrones (Green & Demarque 1987). And in the GW model the post asymptotic giant branch (AGB) stars are not included.

different stellar spectral libraries. We use the BaSeL-2.0 library, which is based on several original grids of model atmosphere spectra: Kurucz (1995, private communication) for O to late-K stars; Fulks et al. (1994) and Bessell et al. (1989, 1991) for M giants in the temperature range 3500–2500 K; and Allard & Hauschildt (1995) for M dwarfs, whereas GW used the theoretical spectra of Kurucz (1992) for stars hotter than 3750 K and composite spectra for cooler stars by patching together model atmospheres (Bessell et al. 1989, 1991, and references therein) and optical observational spectra of M giants Gunn & Stryker (1983).

different IMF shapes. We use the KTG IMF (Kroupa et al. 1993), whereas GW adopt the Salpeter IMF with a slope of = 2.35 (Salpeter 1955), i.e.,

$$(M) = C M^{-2.35} \quad (8)$$

where C is a normalization constant.

The difference between our ISEDs and those of GW can possibly be attributed to either the choice of stellar evolu-

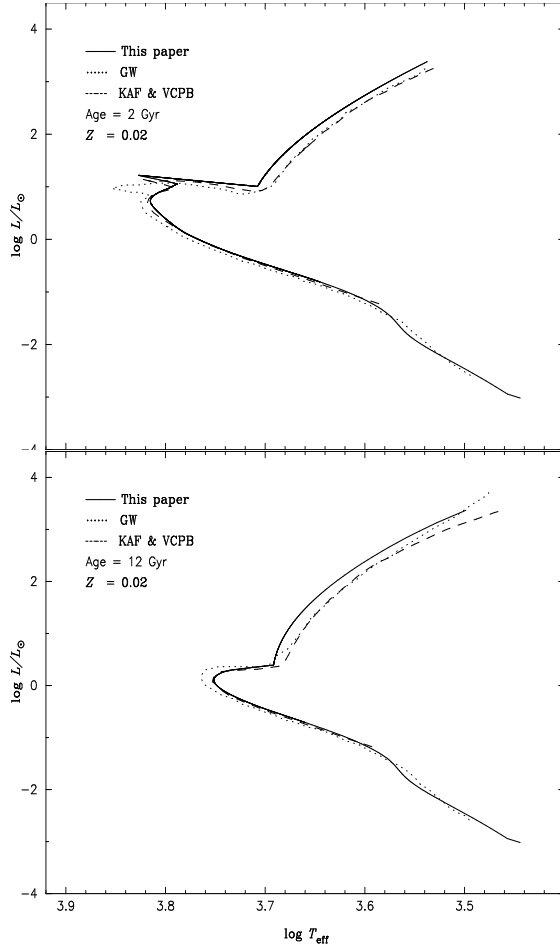


Figure 5. Theoretical isochrones of 2 G yr and 12 G yr old, instantaneous burst stellar populations with solar metallicity. Results from this work, GW, KAF and VCPB are shown.

tional models, the spectral library, the IM F and/or the inclusion of post AGB in EPS model. In the top panels of Figs. 3 and 4 we supplement the ISED drawn from the Salpeter IM F with slope $\beta = 2.35$ and the ISED from the KTG IM F but no themally pulsing giant branch/proto planetary nebula/planetary nebula (TPAGB/PPN/PN, these phases are beyond "early asymptotic giant branch [EAGB]", are collectively termed "post EAGB [PEAGB]" stars included for solar metallicity SSPs at ages of 2 G yr and 12 G yr. In the bottom panels we give the fractional contributions of different evolutionary stage to the total flux for 2 G yr and 12 G yr SSPs of solar metallicity. In it various abbreviations are used to assign the evolution phases. They are as follows: "M S" stands for main-sequence stars, "HG" stands for Hertzsprung gap; "GB" stands for the first giant branch; "CHeB" stands for core helium burning; and the M S is divided into two phases to distinguish deeply or fully convective low-mass stars ($M < 0.7M_{\odot}$) and stars of higher mass with little or no convective envelope ($M > 0.7M_{\odot}$).

(2) Analysis of the Difference of ISEDs in the far-ultraviolet Region

First, the adoption of different spectral libraries can not cause significant discrepancy of ISEDs in the region $\log(\lambda/\text{Å}) < 3.3$. The reason is that the total light in this wavelength region is dominated by PEAGB stars (see the bottom panels of Figs. 3 and 4), in an exact word, by PN stars with temperature $\log(T_e/\text{K}) > 5.0$. For these hotter PN stars the GW model and our model actually use the same spectral library.

Furthermore, the top panels of Figs. 3 and 4 show that (i) the ISED of GW in the far-ultraviolet region agree with our result with the KTG IM F but no PEAGB stars included; (ii) two ISEDs overlap for our SSPs with the different IM F shapes, i.e., the KTG IM F and the Salpeter IM F with a slope of $\beta = 2.35$ in the region $\log(\lambda/\text{Å}) < 3.3$.

Therefore the significant disagreement between our ISED in the region $\log(\lambda/\text{Å}) < 3.3$ and that of GW is dominated by the inclusion of PN stars in PEAGB stage for SSPs, and the IM F shape is not the main factor.

(3) Analysis of the Difference in the Visible and Infra-red Region

From the bottom panel of Fig. 3 we see that the total flux in the visible and infra-red regions is dominated by M S stars with mass $M < 0.7M_{\odot}$, CHeB stars and cooler TPAGB/PPN stars in PEAGB stage (only at wavelength $\log(\lambda/\text{Å}) > 3.9$) for young SSPs ($\tau = 2 \text{ G yr}$). The contribution of M S stars to the light is greater than those of CHeB and the cooler TPAGB/PPN stars in the region of $3.5 < \log(\lambda/\text{Å}) < 4.0$, while the cooler TPAGB/PPN stars make the greatest contribution to the light in the region $4.0 < \log(\lambda/\text{Å}) < 4.2$.

From the bottom panel of Fig. 4 we see that the light in the visible and infra-red regions is dominated by M S stars with mass $M < 0.7M_{\odot}$, CHeB stars and GB stars for old SSPs ($\tau = 12 \text{ G yr}$). The contribution of M S stars and GB stars is greater than that of the other two evolutionary stages at shorter and longer wavelengths, respectively, and the contribution of M S stars to the light is equal to GB at wavelength $\log(\lambda/\text{Å}) = 3.8$.

The top panels of Figs. 3 and 4 show that (i) the inclusion of TPAGB/PPN stars in PEAGB stage in EPS models can produce a significant deviation of ISEDs in the visible and infra-red regions for the young SSPs ($\tau = 2 \text{ G yr}$), but almost no effect for the old SSPs ($\tau = 12 \text{ G yr}$). The reason is that the cooler TPAGB/PPN stars in PEAGB stage contribute a lot to the light for young SSPs at the red end of this region, but almost no light contribution for old SSPs (see the bottom panels of Figs. 3 and 4). The relatively greater contribution of the cooler TPAGB/PPN stars, for young SSPs, is mainly caused by the fact that the relative number of the TPAGB/PPN stars is greater than that for old SSPs. (ii) For $\tau = 2 \text{ G yr}$ SSPs, the ISEDs for SSPs without PEAGB stars included are as much as 1 mag greater than those for SSPs including PEAGB stars. This reason of the blueness of ISEDs is that the SSPs would look like younger and the ISEDs trend to be bluer if omitting those cooler TPAGB/PPN stars in PEAGB stage. (iii) Also for $\tau = 2 \text{ G yr}$ SSPs, the discrepancy in ISEDs arising from the inclusion of TPAGB/PPN stars is larger than that arising from the different models (the GW model and our model).

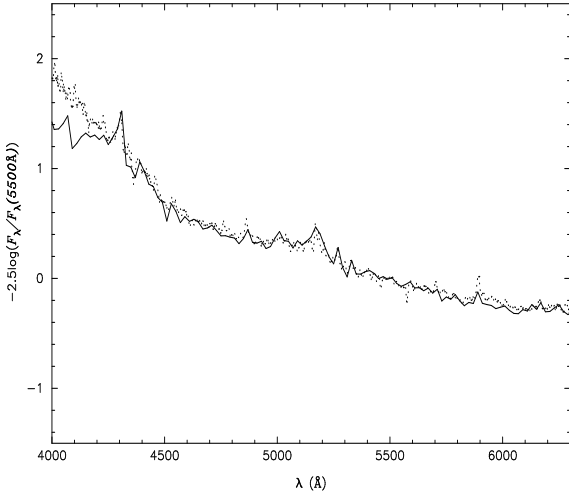


Figure 6. The fit to the ISED of NGC 6838 (dotted line) in the range 4000–6400 Å. The model ISED is for a SSP with solar metallicity and 12.6 G yr (solid line). The flux is expressed in magnitude and is normalized to zero at 5500 Å.

(iv) the adoption of different IMF shapes almost do not affect the ISEDs in the visible and infra-red regions. This can be inferred from the uniqueness of ISEDs between the values with the KTG IMF and those with the Salpeter IMF with slope = 2.35.

Besides the inclusion of PEAGB stars, the adoption of different spectral library and evolutionary models can result in the deviation of ISEDs in the visible and infra-red regions. In Fig. 5 we plot theoretical isochrones for solar-metallicity SSPs at ages of 2 G yr and 12 G yr, as calculated by GW and this work. It reveals three significant deviations between the two isochrones: (i) M S stars with mass $M = 0.7M_{\odot}$ (corresponding roughly to $\log T_{\text{eff}}$ of 3.6) in our models are slightly cooler than that in the GW models; (ii) sub-giant stars in our models are significantly bluer. The cooler M S stars in our models cause redder visible and infra-red continuum, the hotter GB stars cause bluer continuum, and the reddening of ISEDs caused by cooler M S stars is compensated by the hotter GB stars.

In summary the discrepancy between our ISEDs in the visible and infra-red regions and those of GW is not caused mainly by the adoption of different IMF shapes, i.e., the KTG IMF and the Salpeter IMF with a slope of = 2.35, but by the adoption of different stellar evolutionary models and spectral library in EPS model. The inclusion of the cooler TPAB/PNN stars in PEAGB stage can produce a significant deviation of ISEDs for young SSPs, but almost no effect for old SSPs in this region.

3.1.2 Comparison with the ISED of NGC 6838

We compare model ISEDs with that of NGC 6838. The spectral data of NGC 6838 is from Trager et al. (1998) and covers 4000–6400 Å, its resolution is 1.25 Å. The result reveals that NGC 6838 can be fitted by a SSP with solar metallicity and an age of 12.6 G yr. In Fig. 6 we present the ISED of NGC 6838 and the model ISED for an SSP with solar metallicity and an age of 12.6 G yr, the flux is expressed in magnitude and is normalized to zero at 5500 Å. From Fig. 6 we see

that the agreement between model and observed spectrum is quite well in the range $< 4300 \text{ Å}$, but the agreement is not so good for shorter region.

3.2 Lick/IDS absorption feature indices

In Table 1 we present all resulting Lick/IDS spectral absorption feature indices for 7 metallicities from $Z = 0.0001$ to $Z = 0.03$. All indices except for H increase with increasing age and metallicity, and the variation of these indices with age is larger at early age.

3.2.1 Comparison with the results of previous studies

In Fig. 7 we give the evolution of the Lick/IDS spectral absorption feature indices for solar-metallicity SSPs with the KTG IMF, supplemented with the indices for solar-metallicity SSPs obtained by GW (1994), VCPB (1996) and KAF (1999). Except for CN₁, CN₂, Ca4277, NaD, TiO₁ and TiO₂ indices, which show much stronger discrepancies between the studies, all indices agree with those of other studies.

(1) Description of the VCPB and the KAF model

The VCPB model adopts the theoretical isochrones of Bertelli et al. (1994), empirical spectra whenever possible, the fitting functions for CN₁ and CN₂ indices from Vazdekis et al. (1996) and the fitting functions for the other Lick indices from Worthey et al. (1994), and two IMF shapes: unimodal and bimodal. The unimodal IMF takes the form

$$(M) = M^{\alpha} \quad (9)$$

where α for the solar neighborhood is equal to 1.35 and M is a constant. The bimodal IMF is described by

$$(M) = \begin{cases} 0.4 & M = 0.2; \\ p(M) & 0.2 < M < 0.6; \\ M & M = 0.6; \end{cases} \quad (10)$$

where $p(M)$ is a spline. For stars with mass lower than $0.6M_{\odot}$ the tracks are from Pols et al. (1998), as used by us.

KAF used the evolutionary tracks from the Padova group (Bressan et al. 1993; Fagotto et al. 1994a,b,c), for lower masses ($0.08 < M < 0.5M_{\odot}$) used the tracks of Chabrier & Baraffe (1997), theoretical colour calibrations from Lejeune et al. (1997, 1998), fitting functions for stellar atmospheric indices from Worthey et al. (1994), and a Salpeter-like IMF with a slope of 1.35 (Salpeter 1955).

(2) Analysis of the disagreement of Indices amongst those models

In order to investigate which factors cause the difference between our synthetic Lick/IDS absorption-line indices and those of GW, especially in the CN₁, CN₂, Ca4277, NaD, TiO₁ and TiO₂ indices, in Fig. 7 we also give the Lick/IDS absorption feature indices for SSPs with the Salpeter IMF with a slope of = 2.35 and the indices for SSPs with the KTG IMF but no PEAGB stars included in EPS model. It shows that the choice of the IMF and the exclusion of

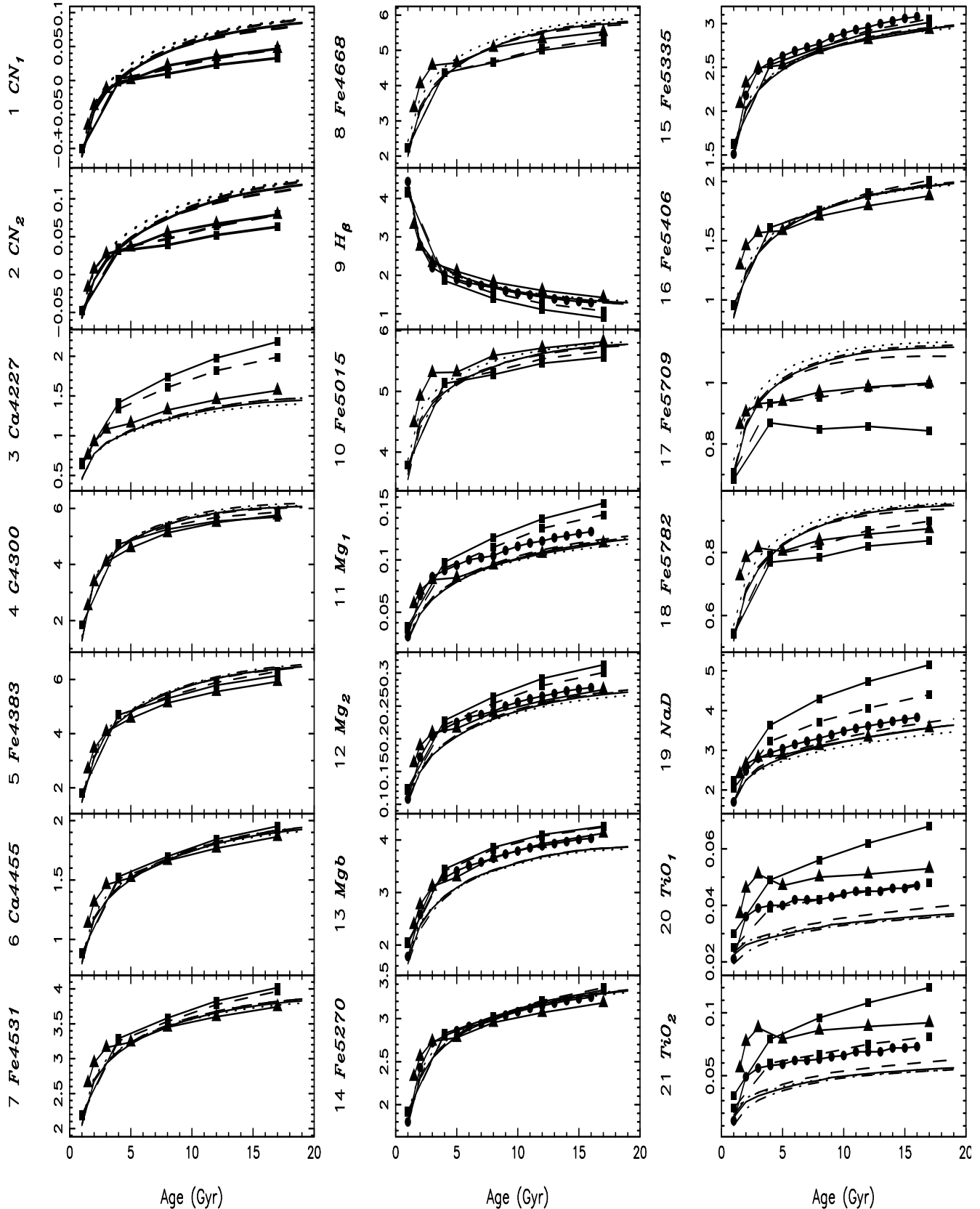


Figure 7. Evolution of absorption indices in Lick/ID S system for solar-metallicity instantaneous burst SSPs, according to several recent EPS models (Worley [1994, solid line + solid triangle], Vazdekis et al. [1996, solid line + solid square for the unimodal IMF, and dashed-line + solid square for the bimodal IMF], and Kurth, Avensleben & Fricke [1999, solid line + solid circle]). Indices for our SSPs drawn from the Salpeter IMF with slopes = 2.35 [dashed line] and 1.35 [dot-dash], and the KTG IMF but no PEAGB stars included [dotted line] are supplemented.

PEAGB stars give rise to only small changes in Fe5406, NaD, TiO₁ and TiO₂ indices, and the deviations introduced by the IMF shape and the exclusion of PEAGB stars are smaller than the discrepancies between the two models. So the disagreement in the Lick/IDS absorption-line indices between our work and the GW model is mainly caused by the adoption of spectral library and stellar evolutionary models. The effects of adopting different stellar evolutionary models on the Lick/IDS indices are as follows: (i) Cooler MS stars with mass $M = 0.7M_{\odot}$ in our models (see Fig. 5) make the absorption-line indices at redder end (NaD, TiO₁, TiO₂) and the blue index Ca4277 higher because these indices decrease sharply with increasing temperature, but make CN₁ and CN₂ lower. (ii) Hotter GB stars in our models (see Fig. 5) make NaD, TiO₁ and TiO₂ and Ca4277 significantly lower, but CN₁ and CN₂ higher. (iii) The effect of cooler MS stars on the Lick/IDS indices is contrary to that of hotter GB stars, and the deviations are dominated by MS stars, the reason is the Lick/IDS indices cover the region 4000–6000 Å (i.e., $3.6 < \log(\text{A}) < 3.8$), in which the total light is dominated by MS stars with mass $M = 0.7M_{\odot}$.

KAF (1999) use the same spectral library (i.e., the BaSeL-2.0 library) and the same fitting functions for Lick/IDS absorption indices (i.e. the functions of Worthey et al., 1994) as those in our model. So the disagreement between our absorption-line indices and those of KAF is possibly introduced by the adoption of different evolutionary models and the IMF shape. In Fig. 7 we give the indices for SSPs with the Salpeter-like IMF with a slope of $\gamma = 1.35$, as used by KAF. It shows that the deviation arising from the IMF shape is smaller than that arising from the different models. So the difference between this work and the KAF models is mainly caused by the choice of stellar evolutionary models. In Fig. 5 the theoretical Padova isochrones used by KAF are given for solar-metallicity SSPs at ages of 2 Gyr and 12 Gyr. It shows that the tracks of MS stars with $M = 0.7M_{\odot}$ in our models agree with those in the KAF models. According to the analysis in the above paragraph, i.e., the deviations are dominated by MS stars with mass $M = 0.7M_{\odot}$, we can draw the following conclusion: the deviations in the Lick/IDS indices between our models and KAF models are smaller than those between our models and GW models, in fact, this conclusion coincides with the comparison of TiO₁ and TiO₂ in Fig. 7.

VCPB (1994) use different stellar evolutionary models, spectral library and two different IMF shapes from those in our models. In Fig. 7 we give the indices from the VCPB models for the unimodal and bimodal IMF with a slope of 2.35. It shows that the significant discrepancies between the unimodal and bimodal models exist in Fe5709, NaD, TiO₁ and TiO₂ indices. Our results are much closer to those with the bimodal IMF than those with the unimodal IMF. The differences between the results in our models and those in the VCPB models are possibly caused by the adoption of different stellar evolutionary models, spectral library and the IMF shape. In fact, the VCPB and KAF models adopt the same isochrones, i.e., Padova isochrones (see Fig. 5), so the deviations of Lick/IDS indices introduced by the different evolutionary models between our and VCPB models, is same as those between our models and KAF models.

Table 2. Manual of Observational data

	NAME	SA	C	O	L	S
1	M 31 4	SA				
2	M 31 23	SA				
3	M 31 42	SA				
4	M 31 76	SA				
5	M 31 87	SA				
6	M 31 95	SA				
7	M 31 99	SA				
8	M 31 100	SA				
9	M 31 116	SA				
10	M 31 196	SA				
11	M 31 282	SA				
12	M 31 301	SA				
13	M 31 M II	SA				
14	M 31 M IV	SA				
15	M 31 V 101	SA				
16	M 31 V 12	SA				
17	M 31 V 64	SA				
18	NGC 2158		C			
19	NGC 5024		C	O		
20	NGC 5272		C	O		
21	NGC 5904		C	O		
22	NGC 6171		C	O		
23	NGC 6205		C	O		
24	NGC 6218		C	O		
25	NGC 6229		C			
26	NGC 6341		C	O		
27	NGC 6356		C	O		
28	NGC 6624			O	L	S
29	NGC 6637		C			
30	NGC 6712		C	O		
31	NGC 6838		C	O		
32	NGC 6981		C			
33	NGC 7006		C			
34	NGC 7078		C	O		
35	NGC 7089		C	O		
36	M 32					

3.2.2 Comparison with observed clusters

As another test, the model indices are checked against a wide variety of available observations. We compare our absorption-line indices with those of Galactic and M 31 globular clusters and those of the circum nuclear region of M 32 in many index-index diagrams (210 diagrams in total, not included in this paper). The line strengths of Galactic and M 31 globular clusters are from Trager et al. (1998) and that of M 32 from del Burgo et al. (2001, references therein). In the database of Trager et al. (1998) 36 globular clusters (18 M 31 and 18 Galactic clusters) are included (see Table 2). M 31 globular clusters are observed with the standard aperture ($1.4'' \times 1.4''$, hereinafter 'SA'). The Galactic globular clusters are observed with a long slit of standard width ($1.4'' \times 16''$) that was raster-scanned on the sky to create a square aperture of size $66'' \times 66''$, this resulted in two square apertures, one centered on the cluster (hereinafter 'C') and one for the "o" beam (hereinafter 'O') located $35''$ to the east. For NGC 6624, the 'L' aperture is $45'' \times 60''$ and the 'S' aperture is $13'' \times 13''$, both are centered on the cluster. Raster scans have the same spectral resolution as standard-slitwidth scans ($1.4''$). In this paper M 31 V 204 has been

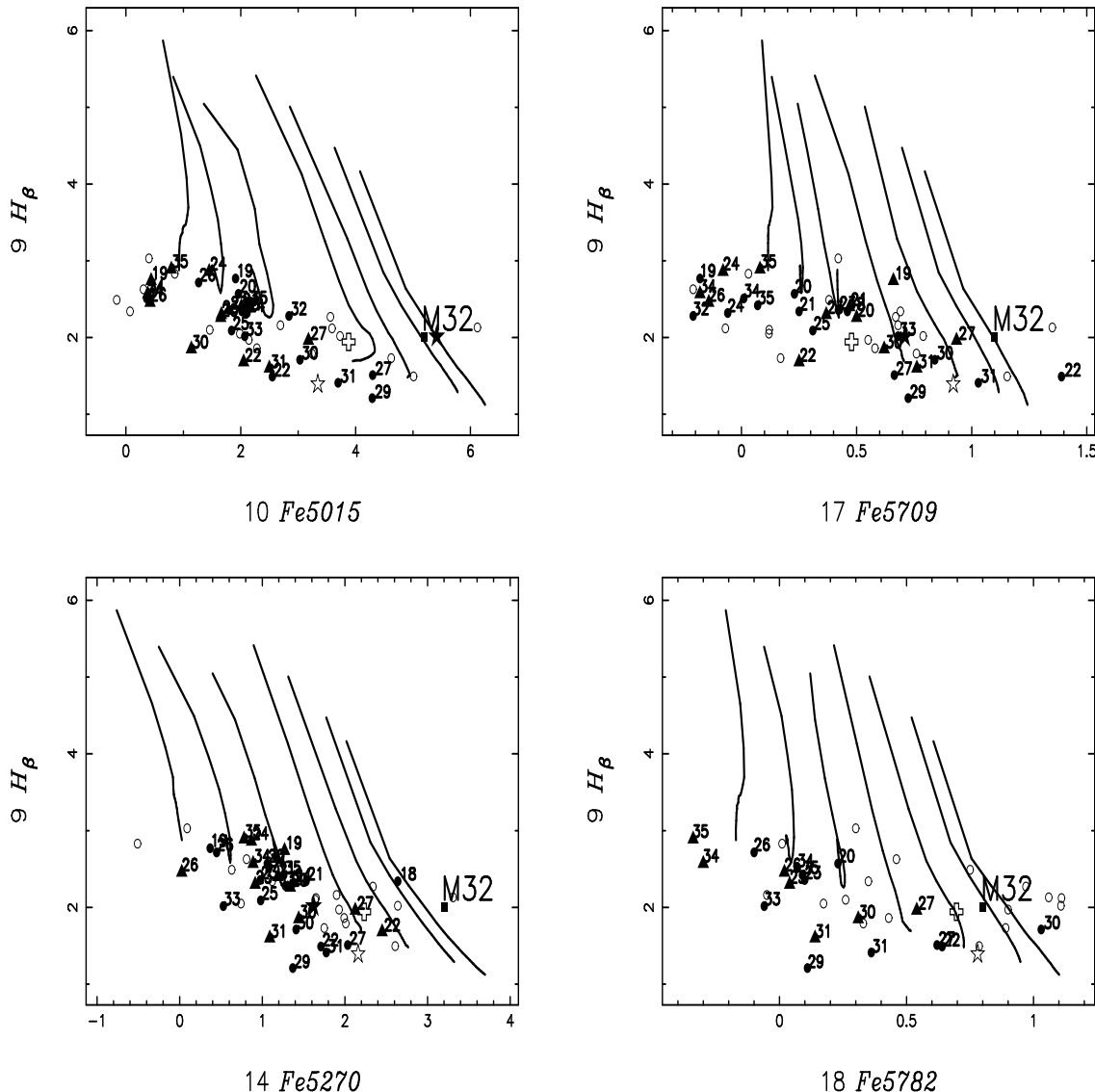


Figure 8. Comparison of our integrated indices with observations of Galactic (solid symbols) and M 31 (open circle) globular clusters. The number indicate the corresponding cluster in Tab. 2. For Galactic cluster, the data for the center ('C') is indicated by solid circle, those for the center ('O') by solid triangle. For Galactic cluster, NGC 6624, the data of 'O', 'L' and 'S' is indicated by solid star, open cross and open star, respectively.

omitted from the database of Trager et al. (1998) because of larger deviation from our models.

The results reveal that our models fit the data very well in many index-index diagrams, while in some index-index diagrams the models do not match real globular clusters well, e.g. in the plots of T_{IO_1} vs. other indices. The index T_{IO_1} is systematically smaller than observations. In Fig. 8 we only give several representative plots in which the model predictions fit the data well, i.e., H_9 vs. four iron lines (Fe5015, Fe5270, Fe5709 and Fe5782). From Fig. 8 we see that there are no significant discrepancies in spectral indices between M 32 and Galactic globular clusters, and the required metallicity is always lower than solar and the age is older than 10 G yr for most of Galactic and M 31 globular clusters. Meanwhile from Fig. 8 we see that the metallicity of the central region of M 32 approaches to solar metallicity.

4 DETERMINATION OF AGE AND METALLICITY

4.1 Merit Function

Our synthetic spectral absorption indices agree better with the values obtained by other authors and fit the observational data very well in most of index-index diagrams, therefore we use these spectral absorption indices to constrain or determine the age and the metallicity for SSP-like assemblies. The method is based on minimizing a chi-squared merit function $F(J)$ between all observed indices and model predictions. The merit function is a measure for the goodness of the fit for observational data. For each model J merit function is defined as:

$$F(J) = \frac{\sum_{i=1}^n W_i \left(\frac{O_i - M_i(J)}{E_i} \right)^2}{\sum_{i=1}^n W_i} \quad (11)$$

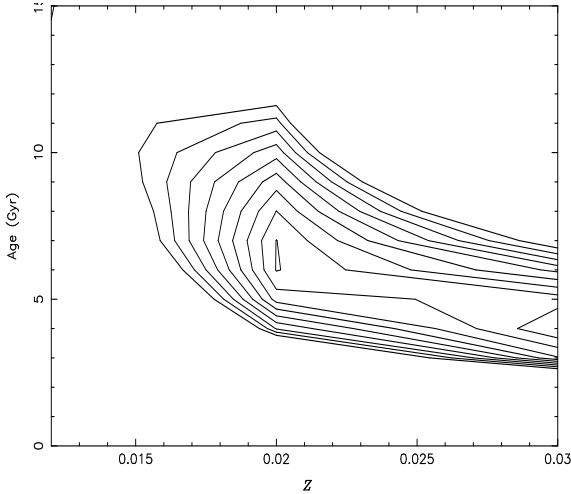


Figure 9. Contours of the merit function of M 32. From center to edge the value of F increase from 1.2 to 2.8 at an interval of 0.2.

where n is the number of observed spectral indices, O_i is the observed value of the i th index, $M_i(J)$ is the synthetic value of corresponding index from model J , and E_i is its observational error, W_i represents its relative weight. In this work we assign the same weight ($\equiv 1$) to all the spectral indices.

4.2 Age and metallicity of M 32

Using the above merit function F we will study the age and the metallicity of the central region of M 32, which is an elliptical galaxy. The reason we discuss M 32 is as follows. Firstly, M 32 is the brightest elliptical galaxy of the Local Group, and has been studied extensively as a template for elliptical galaxies further away. Secondly, the elliptical galaxies can be viewed as SSP-like assemblies because they appear to contain relatively little dust extinction and gaseous interstellar medium (Vazdekis et al. 1996), and in them most of the stars were formed during, or very early after the initial collapse of the galaxy (Bruzual 2003). So we can investigate it by the SSP models.

In Fig. 9 we give its contour map of the merit function F as a function of metallicity Z and age. It shows that the data of absorption indices can be successfully fitted with an instantaneous SSP with an age of 6.5 Gyr and a solar-like metallicity, with F of 1.00 for the central region of M 32.

The age obtained by us is greater than 4 Gyr obtained by del Burgo et al. (2001) from their integral field spectroscopy of the 9×12 arcsec 2 circum nuclear region of M 32 using 30 spectral indices and colours and by Vazdekis & Arimoto (1999) from the blue spectrum using index H , while younger than 7 Gyr obtained by Jones & Worthey (1995) based on their H_{HR} index and 8.5 Gyr from Gilmore et al. (1996) based on their HST analysis resolving M 32 into individual stars.

The resulted metallicity is in full agreement with that of del Burgo et al. (2001) and Vazdekis & Arimoto (1999), both of them predicted solar-like metallicity, but differ from that of Gilmore et al. (1996), who predicted a metallicity of $[\text{Fe}/\text{H}] = -0.25$.

Applying the derived age and metallicity of the central region of M 32 from merit function to the index-index dia-

gram s (see Fig. 9), it seems that the plots of $H - F_{\text{e}5015}$ and $H - F_{\text{e}5782}$ are better diagrams to estimate directly the age and the metallicity from index-index plots. The plots of $H - F_{\text{e}5015}$ and $H - F_{\text{e}5782}$ give the metallicity of $Z > 0.03$ for the center region of M 32.

5 SUMMARY AND CONCLUSION

In this paper we use the EPS technique to present the ISEDs at intermediate resolution (10Å in the ultraviolet and 20Å in the visible) and the Lick/IDS spectral absorption indices for an extensive set of instantaneous burst SSPs of various ages and metallicities (1–19 Gyr, $2.3 \leq [\text{Fe}/\text{H}] \leq 0.2$). In our EPS models we adopted the rapid SSE algorithm, the empirical and semi-empirical calibrated BaSeL-2.0 spectral library and the fitting functions for the absorption-line indices.

As checks on our models, we compare our ISEDs with those of Worthey and the high resolution spectrum of NGC 6838, also compare the Lick/IDS absorption feature indices with the values of other EPS models and those of Galactic and M 31 globular clusters and the central region of M 32. We conclude that: (a) The disagreement between our ISEDs with those of Worthey presents in two wavelength ranges, one in the far-ultraviolet region, the other in the visible and infra-red regions. The discrepancy of ISEDs in the far-ultraviolet region is mainly caused by the inclusion of hotter PN stars in our models, while the discrepancy of ISEDs in the visible and infra-red regions is caused by the choice of stellar evolutionary models and spectral library. The inclusion of cooler T-PAGB/PPN stars can produce a significant deviation in ISEDs for young SSPs, but almost no effect for old SSPs in the visible and infra-red regions. (b) The integrated spectrum of NGC 6838 can be fitted by a SSP with solar metallicity and an age of 12.6 Gyr. (c) When comparing our synthetic Lick/IDS absorption-line indices with the values in the literatures and observational data, we find that our models are generally in agreement with other models and match real globular clusters in most index-index diagrams. T_{IO_1} is, however, systematically smaller.

At last using the merit function F , we find that spectral indices of the central region of M 32 can be fitted with a single stellar population with an age of 6.5 Gyr and a solar-like metallicity with $F = 1.00$. Applying the age and the metallicity of M 32 to some index-index diagrams, we see that $H - F_{\text{e}5015}$ and $H - F_{\text{e}5782}$ are better diagrams to estimate directly the age and metallicity from index-index plots.

ACKNOWLEDGMENTS

We acknowledge the generous support provided by the Chinese Natural Science Foundation (Grant No. 10303006, 19925312 & 10273020), the Chinese Academy of Sciences (KJCX2-SW-T06), Yunnan Natural Science Foundation (Grant No. 2002A 0020Q) and by the 973 scheme (NKBRSF G 1999075406). We are deeply indebted to Dr. Lejeune for making his BaSeL-2.0 model available to us. We also thank Dr P. Podsiadlowski for discussions.

REFERENCES

- Aaronson M., Cohen J. G., Mould J., Malkan M., 1978, *ApJ*, 223, 824
- Allard F., Hauschildt P. H., 1995, *ApJ*, 445, 433
- Arimoto N., 1996, *APS Conf. Ser.* 98, From stars to Galaxies, ed. C. Leitherer, U. Fritz von Alvensleben, & J. Huchra, 287
- Bertelli G., Bressan A., Chiosi C., Fagotto F., Nasi E., 1994, *A&AS*, 106, 275
- Bessell M. S., Brett J. M., Wood P. R., Scholz M., 1989, *A&AS*, 77, 1
- Bessell M. S., Brett J. M., Scholz M., Wood P. R., 1991, *A&AS*, 89, 335
- Bressan A., Fagotto F., Bertelli G., Chiosi C., 1993, *A&AS*, 100, 647
- Bressan A., Chiosi C., Fagotto F., 1994, *ApJS*, 94, 63
- Bressan A., Chiosi C., Tantalo R., 1996, *A&A*, 311, 425
- Bruzual G., 1983, *ApJ*, 273, 105
- Bruzual G., 1996, *RevMexA&A*, 4, 61
- Bruzual G., 2003, in Perez-Fournon I., Balcells M., Moreno-Insertis F., Sanchez F., eds, *Galaxies at High Redshift. XI Canary Islands Winter School of Astrophysics*. Cambridge, Cambridge Univ. Press, 185
- Bruzual G., Charlot S., 1993, *ApJ*, 405, 538
- Buzzoni A., 1989, *ApJS*, 71, 817
- Buzzoni A., 1995, *ApJS*, 98, 69
- Buzzoni A., GaribOLDI G., Mantegazza L., 1992, *AJ*, 103, 1814
- Buzzoni A., Chincarini G., Molinari E., 1993, *ApJ*, 410, 499
- Carraro G., Girardi L., Bressan A., Chiosi C., 1996, *A&A*, 305, 849
- Chabrier G., Baraffe I., 1997, *A&AS*, 327, 1039
- Charbonnel C., Meynet G., Maeder A., Schaller G., Schaerer D., 1993, *A&A*, 101, 415
- del Burgo C., Peletier R. F., Vazdekis A., Arribas S., Mediavilla E., *MNRAS*, 2001, 321, 227
- Eggleton P. P., 1971, *MNRAS*, 151, 351
- Eggleton P. P., 1972, *MNRAS*, 156, 361
- Eggleton P. P., 1973, *MNRAS*, 163, 279
- Fagotto F., Bressan A., Bertelli G., Chiosi C., 1994a, *A&AS*, 104, 365
- Fagotto F., Bressan A., Bertelli G., Chiosi C., 1994b, *A&AS*, 105, 29
- Fagotto F., Bressan A., Bertelli G., Chiosi C., 1994c, *A&AS*, 105, 39
- Flikkum A., Plez B., The P. S., DeWinter D., Westerlund B. E., Steerneman H. C., 1994, *A&AS*, 105, 311
- Frogel J. A., Persson S. E., Cohen J. G., 1980, *ApJ*, 240, 785
- Gunn J. E., Stryker L. L., 1983, *ApJS*, 52, 121
- Gorgas J., Faber S. M., Burstein D., Gonzalez J. J., Courteau S., Rossiter C., 1993, *ApJS*, 86, 153
- Green E. W., Demarque P., King C. R., 1987, *The Revised Yale Isochrones and Luminosity Functions* (New Haven: Yale University Observatory)
- Grimmair C. J., Lauer T. R., Worthey G., Faber S. M., Freedman W. L., Madore B. F., Djorgovski S., Baum W. A., et al., 1996, *AJ*, 112, 1975
- Han Z., Podsiadlowski P., Eggleton P. P., 1994, *MNRAS*, 270, 121
- Hurley J. R., Pols O. R., Tout C. A., 2000, *MNRAS*, 315, 543
- Iben I. Jr., Renzini A., 1983, *ARA&A*, 21, 271
- Jones L. A., Worthey G., 1995, *ApJ*, 446, L31
- Kodama T., Arimoto N., 1997, *A&A*, 320, 41
- Kroupa P., Tout C. A., Gilmore G., 1993, *MNRAS*, 262, 545 (KTG)
- Kurth O. M., Alvensleben U. F.-v., Fricke K. J., 1999, *A&AS*, 138, 19 (KAF)
- Kurucz R. L., 1992, *The Stellar Populations of Galaxies*, IAU Symp. 149, ed. B. Barbuy & A. Renzini (Dordrecht: Kluwer), 225
- Lejeune T., 1997a, Ph.D. thesis, Univ. Louis Pasteur, Strasbourg, France & Astron. Institute of Basel University, Basel, Switzerland
- Lejeune T., Cuisinier F., Buser R., 1997b, *A&AS*, 125, 229
- Lejeune T., Cuisinier F., Buser R., 1998, *A&AS*, 130, 65
- Mould J. R., 1978, *ApJ*, 220, 434
- Mowlavi N., Schaerer D., Meynet G., Bernasconi P. A., Charbonnel C., Maeder A., 1998, *A&AS*, 128, 471
- O'Connell R. W., 1976, *ApJ*, 206, 370
- O'Connell R. W., 1986, in *Stellar Populations*, ed. C. A. Norman, A. Renzini, & M. Tosi (Cambridge: Cambridge Univ. Press), 167
- O'Connell R. W., 1994, in Genzel T., Harris A. I., eds, *NATO Adv. Sci. Inst. Ser. C* 445, *The Neck of Normal Galaxies: Lessons from the Galactic Center*, Dordrecht: Kluwer, P. 255
- Peletier R. F., 1989, Ph.D. thesis, Univ. of Groningen, The Netherlands
- Pols O. R., Tout C. A., Eggleton P. P., Han Z., 1995, *MNRAS*, 274, 964
- Pols O. R., Schroder K. P., Hurley J. R., Tout C. A., Eggleton P. P., 1998, *MNRAS*, 298, 525
- Reimers D., 1975, *Mem. Soc. R. Sci. Liege*, 6e Ser., 8, 369
- Renzini A., 1981, in *Effects of Mass Loss on Stellar Evolution*, ed. C. Chiosi & R. Stahlo (Dordrecht: Reidel), 319
- Renzini A., 1986, in *Stellar Populations*, ed. C. A. Norman, A. Renzini, & M. Tosi (Cambridge: Cambridge Univ. Press), 213
- Rose J. A., 1994, *AJ*, 106, 107
- Salpeter E. E., 1955, *ApJ*, 121, 161
- Schaller G., Schaerer D., Meynet G., Maeder A., 1992, *A&AS*, 96, 269
- Tantalo R., Chiosi C., Bressan A., Fagotto F., 1996, *A&A*, 311, 361
- Tinsley B. M., 1972a, *A&A*, 20, 383
- Tinsley B. M., 1972b, *ApJ*, 178, 39L
- Tinsley B. M., Gunn J. E., 1976, *ApJ*, 203, 52
- Trager S. C., Worthey G., Faber S. M., Burstein D., Gonzalez J. J., 1998, *ApJS*, 116, 1
- Trippico M. J., Bell R. A., 1992, *AJ*, 103, 1285
- VandenBerg D. A., 1985, *ApJS*, 58, 711
- VandenBerg D. A., 1992, *ApJ*, 391, 685
- VandenBerg D. A., Bell R. A., 1985, *ApJS*, 58, 561
- VandenBerg D. A., Laskarides P. G., 1987, *ApJS*, 64, 103
- Vazdekis A., 1999, *ApJ*, 513, 224
- Vazdekis A., 2001, *ApSS*, 276, 839
- Vazdekis A., Arimoto N., 1999, *ApJ*, 525, 144
- Vazdekis A., Casuso E., Peletier R. F., Beckman J. E., 1996, *ApJS*, 106, 307 (VC PB)
- Worthey G., 1992, Ph.D. thesis, Univ. of California, Santa

Cruz

Worley G., 1994, ApJS, 95, 107 (GW)
Worley G., astro.wu.edu/worley/dial/dial.html
Worley G., Ottaviani D.L., 1997, ApJS, 111, 377
Worley G., Faber S.M., González J.J., Burstein D., 1994,
ApJS, 94, 687
Zhang F., Han Z., Li L., Hurley J.R., 2002, MNRAS, 334,
833 (Paper I)

APPENDIX A:

TABLE 1: THE ABSORPTION INDEX FOR SSPSWITH THE KTG IMF (STANDARD MODELS)

Age (G yr)	C N ₁ (mag)	C N ₂ (mag)	C a4277 (A)	G 4300 (A)	F e4383 (A)	C a4455 (A)	F e4531 (A)	F e4668 (A)	H (A)	F e5015 (A)	M g ₁ (mag)
	M g ₂ (mag)	M g _b (A)	F e5270 (A)	F e5335 (A)	F e5406 (A)	F e5709 (A)	F e5782 (A)	N aD (A)	T iO ₁ (mag)	T iO ₂ (mag)	
<i>z = 0.0001</i>											
1.0	-0.114 0.020	0.089 0.447	-0.321 -0.761	-3.184 0.384	-2.013 0.120	-0.026 0.089	-0.237 -0.211	1.208 1.163	5.869 0.014	0.645 0.001	0.010
2.0	-0.307 0.029	-0.098 0.593	-0.170 -0.334	-1.992 0.504	-1.267 0.207	0.070 0.118	0.139 -0.155	0.762 1.147	4.652 0.014	0.959 0.002	0.004
3.0	-0.288 0.031	-0.086 0.608	-0.091 -0.173	-1.322 0.535	-0.873 0.225	0.110 0.130	0.293 -0.141	0.544 1.118	4.082 0.013	1.055 0.001	0.002
4.0	-0.271 0.030	-0.080 0.568	-0.023 -0.080	-0.790 0.542	-0.610 0.224	0.134 0.135	0.386 -0.139	0.374 1.044	3.693 0.012	1.088 0.000	0.001
5.0	-0.271 0.033	-0.087 0.738	0.007 -0.078	-0.669 0.534	-0.503 0.214	0.137 0.129	0.402 -0.144	0.294 0.995	3.595 0.012	1.070 -0.001	0.000
6.0	-0.267 0.034	-0.093 0.796	0.037 -0.074	-0.546 0.529	-0.420 0.207	0.140 0.124	0.415 -0.149	0.218 0.959	3.518 0.011	1.054 -0.002	0.000
7.0	-0.269 0.035	-0.096 0.823	0.053 -0.070	-0.503 0.530	-0.387 0.205	0.142 0.121	0.421 -0.152	0.191 0.953	3.480 0.011	1.044 -0.003	0.000
8.0	-0.270 0.036	-0.099 0.841	0.065 -0.067	-0.495 0.533	-0.357 0.205	0.144 0.120	0.419 -0.155	0.180 0.953	3.463 0.011	1.031 -0.003	0.001
9.0	-0.273 0.036	-0.102 0.848	0.074 -0.068	-0.509 0.533	-0.352 0.204	0.142 0.118	0.413 -0.158	0.171 0.955	3.457 0.011	1.016 -0.003	0.002
10.0	-0.273 0.037	-0.104 0.857	0.084 -0.067	-0.526 0.535	-0.347 0.204	0.141 0.116	0.405 -0.161	0.165 0.963	3.444 0.011	1.000 -0.004	0.003
11.0	-0.274 0.037	-0.105 0.869	0.094 -0.058	-0.531 0.542	-0.321 0.208	0.143 0.116	0.402 -0.162	0.167 0.974	3.416 0.010	0.990 -0.004	0.004
12.0	-0.275 0.038	-0.107 0.872	0.105 -0.046	-0.513 0.548	-0.293 0.211	0.145 0.117	0.403 -0.162	0.163 0.985	3.365 0.010	0.983 -0.004	0.005
13.0	-0.274 0.038	-0.108 0.869	0.115 -0.042	-0.523 0.552	-0.284 0.213	0.145 0.116	0.397 -0.165	0.166 1.000	3.346 0.010	0.970 -0.005	0.006
14.0	-0.275 0.040	-0.109 0.894	0.121 -0.041	-0.530 0.555	-0.295 0.213	0.144 0.115	0.388 -0.168	0.170 1.013	3.323 0.010	0.956 -0.005	0.007
15.0	-0.277 0.041	-0.111 0.900	0.131 -0.033	-0.511 0.563	-0.261 0.218	0.147 0.116	0.384 -0.167	0.183 1.024	3.287 0.010	0.947 -0.005	0.009
16.0	-0.276 0.041	-0.110 0.903	0.142 -0.028	-0.464 0.568	-0.227 0.220	0.149 0.116	0.380 -0.169	0.187 1.038	3.231 0.010	0.935 -0.005	0.010
17.0	-0.273 0.042	-0.109 0.907	0.159 -0.012	-0.358 0.576	-0.160 0.223	0.154 0.116	0.386 -0.170	0.178 1.053	3.130 0.010	0.930 -0.005	0.011
18.0	-0.269 0.044	-0.106 0.944	0.179 0.005	-0.219 0.584	-0.107 0.226	0.160 0.115	0.396 -0.172	0.170 1.070	3.010 0.010	0.926 -0.005	0.012
19.0	-0.151 0.046	0.005 0.983	0.199 0.027	-0.063 0.596	-0.026 0.232	0.168 0.116	0.409 -0.172	0.146 1.084	2.878 0.010	0.925 -0.005	0.013
<i>z = 0.0003</i>											
1.0	-0.037 0.033	0.153 0.645	-0.151 -0.252	-2.139 0.324	-1.376 0.122	-0.034 0.132	0.180 -0.061	0.035 1.109	5.395 0.019	0.823 0.012	0.008
2.0	-0.219 0.044	-0.032 0.706	-0.014 0.173	-1.058 0.500	-0.891 0.225	0.114 0.188	0.602 0.008	-0.058 1.130	4.494 0.021	1.292 0.017	0.006
3.0	-0.204 0.047	-0.020 0.821	0.069 0.354	-0.315 0.572	-0.471 0.266	0.190 0.221	0.798 0.033	-0.112 1.119	3.948 0.020	1.478 0.015	0.005
4.0	-0.199 0.048	-0.018 0.882	0.134 0.480	0.269 0.618	-0.136 0.291	0.247 0.246	0.938 0.049	-0.153 1.098	3.535 0.018	1.600 0.012	0.005
5.0	-0.204 0.048	-0.024 0.950	0.185 0.551	0.737 0.639	0.124 0.297	0.284 0.260	1.025 0.054	-0.207 1.045	3.220 0.017	1.656 0.010	0.004
6.0	-0.210 0.048	-0.032 0.983	0.232 0.027	1.171 0.596	0.378 0.232	0.316 0.116	1.098 -0.172	-0.262 1.084	2.911 0.010	1.697 -0.005	0.003

continued on the next page

Table A 1: continued

A ge (G yr)	C N ₁ (m ag)	C N ₂ (m ag)	C a4277 (A)	G 4300 (A)	F e4383 (A)	C a4455 (A)	F e4531 (A)	F e4668 (A)	H (A)	F e5015 (A)	M g ₁ (m ag)
	M g ₂ (m ag)	M g _b (A)	F e5270 (A)	F e5335 (A)	F e5406 (A)	F e5709 (A)	F e5782 (A)	N aD (A)	T iO ₁ (m ag)	T iO ₂ (m ag)	
	0.049	0.993	0.607	0.657	0.300	0.267	0.057	1.004	0.016	0.008	
7.0	-0.214	-0.038	0.250	1.314	0.478	0.321	1.107	-0.297	2.770	1.683	0.003
	0.050	1.005	0.615	0.659	0.296	0.265	0.055	0.979	0.015	0.006	
8.0	-0.219	-0.044	0.266	1.393	0.546	0.325	1.114	-0.319	2.679	1.673	0.003
	0.051	1.009	0.618	0.661	0.294	0.264	0.052	0.967	0.014	0.005	
9.0	-0.222	-0.047	0.279	1.419	0.582	0.327	1.116	-0.337	2.624	1.662	0.004
	0.052	1.002	0.617	0.661	0.292	0.262	0.049	0.966	0.014	0.004	
10.0	-0.224	-0.050	0.287	1.397	0.721	0.326	1.112	-0.353	2.584	1.648	0.004
	0.053	1.119	0.612	0.659	0.289	0.260	0.045	0.964	0.013	0.003	
11.0	-0.229	-0.054	0.293	1.336	0.726	0.323	1.102	-0.362	2.622	1.629	0.005
	0.053	1.122	0.605	0.658	0.287	0.258	0.042	0.967	0.013	0.002	
12.0	-0.232	-0.057	0.295	1.243	0.689	0.316	1.085	-0.372	2.682	1.606	0.006
	0.052	1.109	0.594	0.653	0.284	0.256	0.037	0.972	0.013	0.002	
13.0	-0.237	-0.061	0.293	1.121	0.642	0.309	1.064	-0.367	2.759	1.584	0.006
	0.052	1.100	0.585	0.653	0.284	0.255	0.036	0.978	0.013	0.001	
14.0	-0.241	-0.064	0.292	1.004	0.582	0.301	1.041	-0.367	2.822	1.561	0.008
	0.052	1.084	0.576	0.651	0.283	0.254	0.032	0.986	0.012	0.001	
15.0	-0.246	-0.069	0.285	0.874	0.537	0.294	1.019	-0.351	2.880	1.541	0.009
	0.052	1.070	0.570	0.653	0.285	0.254	0.032	0.994	0.012	0.000	
16.0	-0.250	-0.072	0.282	0.765	0.487	0.287	0.995	-0.340	2.924	1.518	0.010
	0.052	1.058	0.561	0.651	0.284	0.254	0.028	1.005	0.012	0.000	
17.0	-0.255	-0.075	0.284	0.712	0.474	0.285	0.979	-0.325	2.935	1.501	0.011
	0.051	1.025	0.560	0.654	0.286	0.255	0.026	1.017	0.012	-0.001	
18.0	-0.257	-0.076	0.289	0.716	0.476	0.288	0.973	-0.300	2.914	1.494	0.012
	0.053	1.052	0.567	0.663	0.292	0.256	0.027	1.027	0.012	-0.001	
19.0	-0.258	-0.074	0.303	0.799	0.510	0.294	0.976	-0.289	2.838	1.492	0.014
	0.055	1.085	0.579	0.672	0.296	0.258	0.026	1.042	0.012	-0.001	
<i>z = 0.001</i>											
1.0	-0.140	-0.005	0.029	-1.217	-0.826	0.076	0.655	-0.275	5.046	1.357	0.016
	0.052	0.900	0.399	0.512	0.258	0.244	0.121	1.249	0.029	0.032	
2.0	-0.132	-0.010	0.174	-0.460	-0.552	0.218	0.995	-0.154	4.447	1.945	0.014
	0.059	1.191	0.670	0.661	0.338	0.285	0.140	1.150	0.036	0.044	
3.0	-0.114	-0.004	0.318	0.797	0.145	0.371	1.339	-0.092	3.679	2.245	0.013
	0.067	1.325	0.909	0.794	0.413	0.332	0.179	1.148	0.033	0.040	
4.0	-0.098	0.006	0.395	1.500	0.615	0.453	1.513	-0.023	3.214	2.325	0.014
	0.072	1.386	1.033	0.885	0.470	0.359	0.208	1.193	0.032	0.037	
5.0	-0.087	0.012	0.456	2.081	1.019	0.525	1.650	0.074	2.841	2.457	0.016
	0.077	1.474	1.147	0.965	0.523	0.383	0.232	1.238	0.031	0.036	
6.0	-0.079	0.018	0.503	2.447	1.319	0.573	1.736	0.145	2.601	2.524	0.017
	0.082	1.545	1.223	1.030	0.567	0.397	0.250	1.290	0.030	0.034	
7.0	-0.075	0.020	0.531	2.722	1.487	0.600	1.786	0.151	2.423	2.566	0.018
	0.084	1.563	1.265	1.057	0.590	0.409	0.257	1.306	0.028	0.032	
8.0	-0.078	0.016	0.533	2.857	1.563	0.607	1.797	0.113	2.326	2.556	0.018
	0.084	1.556	1.275	1.053	0.589	0.417	0.257	1.289	0.026	0.027	
9.0	-0.084	0.010	0.526	2.903	1.585	0.607	1.795	0.076	2.281	2.534	0.018
	0.084	1.531	1.274	1.041	0.581	0.421	0.256	1.274	0.024	0.023	
10.0	-0.089	0.005	0.515	2.897	1.570	0.601	1.784	0.032	2.264	2.506	0.018
	0.085	1.510	1.266	1.024	0.568	0.423	0.253	1.259	0.022	0.020	
11.0	-0.097	-0.002	0.501	2.846	1.531	0.593	1.769	-0.009	2.270	2.475	0.018
	0.084	1.471	1.255	1.005	0.554	0.423	0.250	1.247	0.021	0.018	
12.0	-0.108	-0.013	0.484	2.742	1.490	0.577	1.739	-0.063	2.295	2.426	0.018
	0.083	1.438	1.234	0.984	0.537	0.422	0.244	1.230	0.019	0.015	
13.0	-0.112	-0.017	0.473	2.636	1.595	0.569	1.725	-0.087	2.328	2.404	0.018
	0.082	1.486	1.223	0.952	0.507	0.421	0.242	1.233	0.019	0.014	

continued on the next page

Table A 1: continued

Age (G yr)	C N ₁ (mag)	C N ₂ (mag)	C a4277 (A)	G 4300 (A)	F e4383 (A)	C a4455 (A)	F e4531 (A)	F e4668 (A)	H (A)	F e5015 (A)	M g ₁ (mag)
	M g ₂ (mag)	M g _b (A)	F e5270 (A)	F e5335 (A)	F e5406 (A)	F e5709 (A)	F e5782 (A)	N aD (A)	T iO ₁ (mag)	T iO ₂ (mag)	
14.0	-0.118	-0.021	0.470	2.504	1.541	0.559	1.705	-0.114	2.409	2.379	0.019
	0.082	1.496	1.210	0.944	0.503	0.420	0.239	1.235	0.018	0.012	
15.0	-0.123	-0.025	0.466	2.348	1.473	0.547	1.681	-0.140	2.501	2.348	0.020
	0.082	1.505	1.197	0.938	0.500	0.420	0.236	1.241	0.017	0.011	
16.0	-0.130	-0.031	0.451	2.128	1.372	0.527	1.641	-0.168	2.627	2.305	0.020
	0.083	1.502	1.174	0.927	0.494	0.417	0.234	1.244	0.017	0.010	
17.0	-0.137	-0.036	0.436	1.909	1.264	0.507	1.599	-0.197	2.739	2.264	0.021
	0.083	1.495	1.153	0.916	0.489	0.416	0.230	1.247	0.016	0.009	
18.0	-0.144	-0.042	0.421	1.703	1.181	0.490	1.563	-0.205	2.827	2.230	0.022
	0.083	1.494	1.139	0.910	0.487	0.416	0.228	1.254	0.016	0.008	
19.0	-0.152	-0.048	0.414	1.561	1.123	0.480	1.535	-0.208	2.881	2.201	0.022
	0.083	1.499	1.130	0.908	0.487	0.416	0.226	1.262	0.015	0.007	
<i>z = 0.004</i>											
1.0	-0.182	-0.110	0.197	-0.812	-0.327	0.252	1.117	-0.009	5.412	2.266	0.012
	0.067	1.324	0.896	0.695	0.316	0.319	0.214	1.283	0.038	0.046	
2.0	-0.126	-0.071	0.370	0.988	0.521	0.526	1.644	0.460	4.130	3.058	0.014
	0.083	1.599	1.311	0.963	0.514	0.465	0.305	1.224	0.036	0.042	
3.0	-0.089	-0.044	0.496	2.228	1.315	0.708	1.965	0.905	3.256	3.465	0.019
	0.096	1.834	1.575	1.163	0.652	0.540	0.366	1.320	0.034	0.039	
4.0	-0.064	-0.026	0.580	3.017	1.861	0.826	2.160	1.198	2.739	3.711	0.024
	0.105	1.980	1.741	1.294	0.746	0.589	0.406	1.394	0.032	0.038	
5.0	-0.049	-0.014	0.641	3.528	2.231	0.906	2.290	1.394	2.423	3.878	0.028
	0.112	2.087	1.853	1.383	0.812	0.625	0.434	1.451	0.032	0.037	
6.0	-0.038	-0.005	0.687	3.877	2.486	0.967	2.384	1.553	2.229	4.024	0.031
	0.117	2.171	1.936	1.450	0.862	0.648	0.454	1.502	0.033	0.039	
7.0	-0.033	-0.001	0.722	4.075	2.616	1.003	2.436	1.642	2.134	4.115	0.033
	0.121	2.221	1.982	1.491	0.889	0.656	0.462	1.548	0.033	0.041	
8.0	-0.027	0.004	0.763	4.285	2.744	1.044	2.492	1.751	2.050	4.241	0.035
	0.124	2.282	2.034	1.536	0.917	0.662	0.468	1.601	0.035	0.044	
9.0	-0.023	0.006	0.790	4.444	2.857	1.071	2.532	1.799	1.978	4.294	0.037
	0.129	2.358	2.069	1.567	0.938	0.671	0.474	1.639	0.035	0.045	
10.0	-0.021	0.008	0.809	4.571	2.944	1.091	2.562	1.814	1.917	4.319	0.039
	0.132	2.407	2.095	1.589	0.956	0.679	0.479	1.669	0.035	0.045	
11.0	-0.019	0.009	0.824	4.674	3.014	1.108	2.587	1.812	1.865	4.332	0.041
	0.135	2.441	2.116	1.607	0.970	0.687	0.482	1.696	0.035	0.044	
12.0	-0.018	0.009	0.836	4.762	3.068	1.121	2.606	1.791	1.818	4.333	0.043
	0.137	2.465	2.132	1.622	0.982	0.695	0.484	1.719	0.034	0.044	
13.0	-0.019	0.008	0.856	4.805	3.188	1.135	2.630	1.841	1.788	4.304	0.045
	0.141	2.539	2.156	1.657	1.002	0.696	0.491	1.784	0.034	0.044	
14.0	-0.019	0.007	0.872	4.839	3.291	1.146	2.650	1.876	1.764	4.268	0.047
	0.144	2.598	2.175	1.686	1.018	0.697	0.497	1.840	0.034	0.043	
15.0	-0.020	0.007	0.883	4.868	3.371	1.153	2.666	1.882	1.742	4.222	0.049
	0.147	2.631	2.188	1.706	1.031	0.698	0.502	1.884	0.033	0.042	
16.0	-0.020	0.006	0.886	4.888	3.431	1.155	2.676	1.856	1.722	4.157	0.051
	0.148	2.633	2.194	1.719	1.041	0.702	0.507	1.917	0.032	0.040	
17.0	-0.021	0.005	0.888	4.906	3.479	1.156	2.683	1.826	1.702	4.088	0.052
	0.151	2.640	2.197	1.729	1.049	0.704	0.511	1.947	0.030	0.037	
18.0	-0.022	0.004	0.887	4.889	3.526	1.152	2.686	1.792	1.702	4.011	0.054
	0.152	2.631	2.196	1.737	1.055	0.704	0.514	1.977	0.029	0.035	
19.0	-0.022	0.004	0.884	4.886	3.540	1.149	2.688	1.750	1.692	3.950	0.054
	0.154	2.624	2.192	1.739	1.058	0.705	0.517	1.995	0.028	0.033	
<i>z = 0.01</i>											
1.0	-0.150	-0.088	0.305	0.242	0.491	0.504	1.575	0.664	5.007	2.855	0.014

continued on the next page

Table A 1: continued

A ge (G yr)	C N ₁ (m ag)	C N ₂ (m ag)	C a4277 (A)	G 4300 (A)	F e4383 (A)	C a4455 (A)	F e4531 (A)	F e4668 (A)	H (A)	F e5015 (A)	M g ₁ (m ag)
	M g ₂ (m ag)	M g _b (A)	F e5270 (A)	F e5335 (A)	F e5406 (A)	F e5709 (A)	F e5782 (A)	N aD (A)	T iO ₁ (m ag)	T iO ₂ (m ag)	
	0.078	1.375	1.315	1.000	0.536	0.536	0.354	1.254	0.024	0.018	
2.0	-0.075	-0.032	0.583	2.560	2.011	0.888	2.253	1.925	3.286	3.857	0.027
	0.115	2.022	1.887	1.506	0.880	0.676	0.508	1.650	0.029	0.031	
3.0	-0.042	-0.005	0.708	3.605	2.833	1.063	2.537	2.467	2.606	4.212	0.039
	0.134	2.252	2.136	1.728	1.050	0.762	0.578	1.837	0.028	0.031	
4.0	-0.027	0.007	0.774	4.011	3.230	1.147	2.672	2.718	2.349	4.365	0.046
	0.145	2.394	2.257	1.839	1.141	0.806	0.617	1.947	0.028	0.032	
5.0	-0.015	0.018	0.829	4.367	3.606	1.218	2.785	2.927	2.177	4.487	0.051
	0.154	2.501	2.354	1.929	1.214	0.839	0.646	2.038	0.028	0.033	
6.0	-0.007	0.025	0.871	4.590	3.831	1.269	2.865	3.068	2.061	4.573	0.056
	0.162	2.605	2.424	1.995	1.268	0.862	0.668	2.109	0.028	0.034	
7.0	0.000	0.031	0.901	4.730	3.992	1.310	2.929	3.185	1.979	4.647	0.060
	0.168	2.674	2.480	2.048	1.314	0.879	0.687	2.169	0.029	0.036	
8.0	0.002	0.034	0.923	4.816	4.086	1.332	2.963	3.229	1.929	4.677	0.062
	0.172	2.719	2.510	2.077	1.336	0.887	0.693	2.213	0.029	0.036	
9.0	0.007	0.038	0.950	4.963	4.225	1.364	3.011	3.305	1.857	4.728	0.065
	0.177	2.788	2.550	2.114	1.365	0.897	0.702	2.264	0.029	0.037	
10.0	0.012	0.042	0.976	5.107	4.361	1.396	3.057	3.375	1.787	4.779	0.068
	0.182	2.852	2.590	2.151	1.393	0.906	0.710	2.312	0.030	0.038	
11.0	0.016	0.045	1.000	5.227	4.465	1.422	3.094	3.427	1.728	4.820	0.070
	0.186	2.913	2.623	2.181	1.415	0.913	0.716	2.356	0.030	0.038	
12.0	0.018	0.047	1.016	5.305	4.549	1.442	3.121	3.455	1.684	4.848	0.072
	0.189	2.950	2.647	2.204	1.432	0.918	0.719	2.396	0.030	0.039	
13.0	0.020	0.048	1.033	5.386	4.622	1.461	3.149	3.474	1.641	4.875	0.074
	0.192	2.978	2.672	2.226	1.449	0.924	0.722	2.432	0.030	0.039	
14.0	0.022	0.050	1.047	5.458	4.685	1.478	3.172	3.496	1.600	4.899	0.076
	0.195	3.018	2.691	2.245	1.463	0.927	0.724	2.467	0.031	0.040	
15.0	0.022	0.050	1.058	5.506	4.731	1.492	3.190	3.498	1.569	4.918	0.078
	0.198	3.045	2.709	2.263	1.475	0.931	0.725	2.500	0.031	0.041	
16.0	0.023	0.050	1.069	5.558	4.768	1.505	3.207	3.492	1.537	4.936	0.080
	0.200	3.065	2.725	2.277	1.486	0.935	0.726	2.529	0.031	0.041	
17.0	0.023	0.050	1.076	5.601	4.792	1.516	3.221	3.470	1.506	4.951	0.082
	0.202	3.071	2.738	2.289	1.495	0.939	0.726	2.556	0.031	0.041	
18.0	0.018	0.045	1.100	5.607	4.892	1.527	3.242	3.521	1.496	4.922	0.084
	0.205	3.159	2.754	2.321	1.507	0.933	0.725	2.627	0.031	0.042	
19.0	0.016	0.043	1.118	5.625	4.957	1.537	3.260	3.547	1.480	4.905	0.086
	0.207	3.219	2.766	2.344	1.517	0.929	0.725	2.680	0.031	0.043	
z = 0.02											
1.0	-0.112	-0.057	0.464	1.277	1.462	0.800	2.046	2.048	4.472	3.634	0.023
	0.104	1.709	1.774	1.494	0.848	0.698	0.520	1.700	0.022	0.017	
2.0	-0.046	-0.007	0.773	3.418	3.088	1.170	2.678	3.326	2.846	4.483	0.048
	0.149	2.368	2.310	2.016	1.217	0.857	0.673	2.252	0.026	0.029	
3.0	-0.017	0.018	0.906	4.138	3.986	1.327	2.931	3.905	2.414	4.797	0.062
	0.175	2.698	2.540	2.236	1.392	0.933	0.746	2.513	0.027	0.034	
4.0	0.000	0.034	0.989	4.534	4.427	1.425	3.086	4.266	2.189	4.985	0.071
	0.191	2.922	2.681	2.369	1.502	0.977	0.789	2.675	0.029	0.037	
5.0	0.014	0.047	1.057	4.836	4.774	1.504	3.208	4.542	2.023	5.128	0.079
	0.204	3.091	2.788	2.472	1.585	1.009	0.822	2.806	0.030	0.040	
6.0	0.025	0.058	1.118	5.084	5.059	1.569	3.309	4.767	1.893	5.244	0.085
	0.214	3.230	2.875	2.554	1.653	1.032	0.847	2.916	0.031	0.042	
7.0	0.034	0.066	1.166	5.270	5.283	1.621	3.387	4.941	1.794	5.328	0.090
	0.223	3.337	2.941	2.618	1.704	1.050	0.866	3.003	0.031	0.045	
8.0	0.042	0.074	1.206	5.423	5.473	1.666	3.455	5.090	1.712	5.403	0.094
	0.230	3.422	2.999	2.672	1.749	1.065	0.882	3.076	0.032	0.046	

continued on the next page

Table A 1: continued

Age (G yr)	C N ₁ (mag)	C N ₂ (mag)	C a4277 (A)	G 4300 (A)	F e4383 (A)	C a4455 (A)	F e4531 (A)	F e4668 (A)	H (A)	F e5015 (A)	M g ₁ (mag)
	M g ₂ (mag)	M g _b (A)	F e5270 (A)	F e5335 (A)	F e5406 (A)	F e5709 (A)	F e5782 (A)	N aD (A)	T iO ₁ (mag)	T iO ₂ (mag)	
9.0	0.049	0.081	1.246	5.555	5.641	1.708	3.518	5.228	1.641	5.480	0.098
	0.237	3.492	3.052	2.722	1.787	1.077	0.897	3.148	0.033	0.049	
10.0	0.055	0.087	1.280	5.666	5.791	1.743	3.570	5.335	1.577	5.532	0.101
	0.242	3.567	3.097	2.764	1.820	1.086	0.908	3.214	0.034	0.050	
11.0	0.061	0.093	1.311	5.754	5.917	1.775	3.616	5.428	1.526	5.581	0.104
	0.248	3.628	3.135	2.799	1.849	1.094	0.917	3.274	0.034	0.051	
12.0	0.066	0.098	1.341	5.836	6.033	1.804	3.659	5.513	1.477	5.623	0.107
	0.252	3.684	3.172	2.834	1.877	1.101	0.925	3.332	0.034	0.051	
13.0	0.069	0.102	1.366	5.894	6.128	1.829	3.694	5.580	1.438	5.661	0.110
	0.256	3.725	3.202	2.861	1.898	1.105	0.931	3.385	0.035	0.053	
14.0	0.073	0.105	1.387	5.944	6.210	1.851	3.725	5.632	1.403	5.688	0.112
	0.260	3.763	3.229	2.886	1.917	1.109	0.936	3.434	0.035	0.053	
15.0	0.076	0.109	1.405	5.982	6.278	1.870	3.752	5.679	1.374	5.714	0.114
	0.263	3.797	3.252	2.907	1.934	1.112	0.940	3.480	0.036	0.054	
16.0	0.078	0.111	1.420	6.013	6.337	1.887	3.776	5.716	1.348	5.736	0.115
	0.265	3.822	3.274	2.926	1.949	1.114	0.943	3.523	0.036	0.054	
17.0	0.080	0.114	1.429	6.029	6.385	1.900	3.795	5.744	1.327	5.752	0.117
	0.268	3.839	3.291	2.941	1.961	1.115	0.945	3.562	0.036	0.055	
18.0	0.083	0.116	1.440	6.056	6.431	1.914	3.815	5.769	1.305	5.766	0.118
	0.270	3.854	3.309	2.957	1.972	1.117	0.947	3.600	0.037	0.056	
19.0	0.085	0.118	1.445	6.067	6.466	1.925	3.830	5.783	1.289	5.776	0.120
	0.271	3.864	3.323	2.971	1.983	1.117	0.948	3.635	0.037	0.056	
z = 0.03											
1.0	-0.094	-0.044	0.565	1.841	1.973	0.975	2.299	2.910	4.163	4.076	0.031
	0.120	1.872	2.019	1.805	1.031	0.796	0.606	2.003	0.022	0.018	
2.0	-0.029	0.007	0.886	3.954	3.861	1.346	2.919	4.252	2.637	4.873	0.061
	0.172	2.599	2.542	2.329	1.415	0.963	0.756	2.599	0.026	0.030	
3.0	-0.004	0.029	1.045	4.534	4.689	1.499	3.170	4.842	2.285	5.173	0.079
	0.202	3.026	2.771	2.564	1.597	1.036	0.832	2.917	0.029	0.039	
4.0	0.011	0.044	1.150	4.821	5.082	1.594	3.326	5.194	2.087	5.343	0.090
	0.221	3.266	2.909	2.706	1.709	1.076	0.879	3.124	0.031	0.045	
5.0	0.024	0.057	1.242	5.078	5.427	1.677	3.459	5.497	1.923	5.484	0.100
	0.237	3.464	3.023	2.822	1.801	1.109	0.915	3.289	0.033	0.050	
6.0	0.035	0.068	1.320	5.293	5.716	1.747	3.568	5.746	1.791	5.600	0.108
	0.250	3.624	3.114	2.914	1.874	1.132	0.942	3.423	0.034	0.054	
7.0	0.045	0.077	1.388	5.455	5.953	1.805	3.659	5.952	1.690	5.695	0.115
	0.261	3.751	3.190	2.991	1.934	1.150	0.964	3.538	0.036	0.057	
8.0	0.053	0.085	1.442	5.574	6.142	1.852	3.732	6.119	1.611	5.772	0.120
	0.269	3.850	3.252	3.051	1.982	1.165	0.983	3.631	0.037	0.059	
9.0	0.061	0.094	1.495	5.664	6.311	1.897	3.803	6.286	1.543	5.848	0.126
	0.278	3.937	3.311	3.110	2.028	1.177	1.002	3.721	0.038	0.063	
10.0	0.069	0.103	1.553	5.764	6.490	1.943	3.873	6.443	1.471	5.925	0.131
	0.286	4.029	3.372	3.166	2.074	1.192	1.020	3.813	0.039	0.065	
11.0	0.076	0.110	1.602	5.840	6.638	1.981	3.932	6.569	1.412	5.984	0.135
	0.293	4.114	3.422	3.213	2.111	1.202	1.033	3.895	0.039	0.066	
12.0	0.083	0.118	1.649	5.905	6.778	2.017	3.986	6.686	1.358	6.038	0.139
	0.300	4.184	3.468	3.256	2.145	1.211	1.046	3.972	0.040	0.067	
13.0	0.090	0.125	1.695	5.964	6.907	2.051	4.038	6.795	1.308	6.088	0.143
	0.306	4.249	3.513	3.296	2.177	1.220	1.057	4.046	0.040	0.068	
14.0	0.096	0.132	1.734	6.002	7.022	2.081	4.084	6.889	1.267	6.128	0.147
	0.311	4.306	3.552	3.334	2.207	1.227	1.068	4.115	0.041	0.069	
15.0	0.101	0.137	1.771	6.040	7.118	2.108	4.124	6.967	1.229	6.165	0.150
	0.316	4.352	3.586	3.363	2.230	1.231	1.075	4.179	0.041	0.070	
16.0	0.105	0.142	1.801	6.059	7.200	2.130	4.158	7.033	1.200	6.196	0.152

continued on the next page

Table A 1: continued

A ge (G yr)	C N ₁ (mag)	C N ₂ (mag)	C a4277 (A)	G 4300 (A)	F e4383 (A)	C a4455 (A)	F e4531 (A)	F e4668 (A)	H (A)	F e5015 (A)	M g ₁ (mag)
	M g ₂ (mag)	M g _b (A)	F e5270 (A)	F e5335 (A)	F e5406 (A)	F e5709 (A)	F e5782 (A)	N aD (A)	T iO ₁ (mag)	T iO ₂ (mag)	
17.0	0.320	4.394	3.616	3.390	2.251	1.234	1.082	4.238	0.042	0.071	
	0.110	0.148	1.832	6.083	7.283	2.153	4.193	7.101	1.168	6.222	0.155
	0.324	4.431	3.646	3.415	2.271	1.237	1.089	4.296	0.042	0.072	
18.0	0.114	0.153	1.856	6.088	7.353	2.171	4.222	7.150	1.145	6.238	0.157
	0.327	4.456	3.672	3.437	2.288	1.240	1.095	4.351	0.042	0.072	
19.0	0.119	0.158	1.877	6.094	7.419	2.188	4.250	7.202	1.123	6.255	0.159
	0.330	4.480	3.697	3.457	2.304	1.242	1.101	4.402	0.042	0.072	

This paper has been typeset from a \TeX / \LaTeX file prepared by the author.